



# More severe hydrological drought events emerge at different warming levels over the Wudinghe watershed in northern China

Yang Jiao<sup>1,2</sup> and Xing Yuan<sup>1,2</sup>

<sup>1</sup>School of Hydrology and Water Resources, Nanjing University of Information Science and Technology, Nanjing, 210044, Jiangsu, China

<sup>2</sup>Key Laboratory of Regional Climate-Environment for Temperate East Asia (RCE-TEA), Institute of Atmospheric Physics, Chinese Academy of Sciences, Beijing, 100029, China

**Correspondence:** Xing Yuan (xyuan@nuist.edu.cn)

Received: 8 May 2018 – Discussion started: 16 July 2018

Revised: 25 December 2018 – Accepted: 19 January 2019 – Published: 1 February 2019

**Abstract.** Assessment of changes in hydrological droughts at specific warming levels is important for an adaptive water resources management with consideration of the 2015 Paris Agreement. However, most studies focused on the response of drought frequency to the warming and neglected other drought characteristics, including severity. By using a semi-arid watershed in northern China (i.e., Wudinghe) as an example, here we show less frequent but more severe hydrological drought events emerge at 1.5, 2 and 3 °C warming levels. We used meteorological forcings from eight Coupled Model Intercomparison Project Phase 5 climate models under four representative concentration pathways, to drive a newly developed land surface hydrological model to simulate streamflow, and analyzed historical and future hydrological drought characteristics based on the standardized streamflow index. The Wudinghe watershed will reach the 1.5, 2 and 3 °C warming levels around 2015–2034, 2032–2051 and 2060–2079, with an increase in precipitation of 8%, 9% and 18% and runoff of 27%, 19% and 44%, and a drop in hydrological drought frequency of 11%, 26% and 23% as compared to the baseline period (1986–2005). However, the drought severity will rise dramatically by 184%, 116% and 184%, which is mainly caused by the increased variability in precipitation and evapotranspiration. The climate models and the land surface hydrological model contribute to more than 80% of total uncertainties in the future projection of precipitation and hydrological droughts. This study suggests that different aspects of hydrological droughts should be carefully investigated when assessing the impact of 1.5, 2 and 3 °C global warming.

## 1 Introduction

Global warming has affected both natural and artificial systems across continents, bringing a lot of ecohydrological crises to many countries (Gitay et al., 2002; Tirado et al., 2010; Thornton et al., 2014). The Intergovernmental Panel on Climate Change (IPCC) Fifth Assessment Report (AR5) concluded that global average surface air temperature increased by 0.61 °C in 1986–2005 compared to preindustrial periods (IPCC, 2014a). In order to mitigate global warming, the Conference of the Parties of the United Nations Framework Convention on Climate Change (UNFCCC) emphasized in the Paris Agreement that the increase in global average temperature should be controlled within 2 °C above preindustrial levels, and further efforts should be made to limit it below 1.5 °C. However, whether the temperature controlling goal can be reached is still unknown, with much difficulty under current emission conditions (Peters et al., 2012). In addition, a specific warming level such as 2 °C increase would be too high for many regions and countries (James et al., 2017; Rogelj et al., 2015). Therefore, it is necessary to assess changes in the regional hydrological cycle and extremes under 1.5, 2 and even 3 °C global warming.

Global warming is mainly caused by greenhouse gases emissions and has a profound influence on hydrosphere and ecosphere (Barnett et al., 2005; Vorosmarty et al., 2000). It alters the hydrological cycle both directly (e.g., influences precipitation and evapotranspiration) and indirectly (e.g., influences plant growth and related hydrological processes) at global (Zhu et al., 2016; McVicar et al., 2012) and local scales (Tang et al., 2013; Zheng et al., 2009; Zhang et al.,

2008). Besides affecting the mean states of the hydrological conditions, global warming also intensifies hydrological extremes significantly, such as droughts which were regarded as naturally occurring events when water (precipitation, or streamflow, etc.) is significantly below normal over a period of time (Van Loon et al., 2016; Dai, 2011). Among different types of droughts, hydrological droughts focus on the decrease in the availability of water resources, e.g., surface and/or ground water (Lorenzo-Lacruz et al., 2013). Many researchers paid attention to the historical changes, future evolutions and uncertainties, and causing factors for hydrological droughts (Chang et al., 2016; Kormos et al., 2016; Orłowsky and Seneviratne, 2013; Parajka et al., 2016; Perez et al., 2011; Prudhomme et al., 2014; Van Loon and Laaha, 2015; Wanders and Wada, 2015; Yuan et al., 2017). Most drought projection studies focused on the future changes over a fixed time period (e.g., late 21st century), but recent studies pointed out the importance on hydrological drought evolution at certain warming levels (Roudier et al., 2016; Marx et al., 2018) given the aim of the Paris Agreement. Moreover, the changes in characteristics (e.g., frequency, duration, severity) of hydrological drought events at specific warming levels received less attention. The projection of these drought characteristics could provide more relevant guidelines for policymakers on implementing adaptation strategies.

In the past 5 decades, a significant decrease in channel discharge was observed in the middle reaches of the Yellow River basin over northern China (Yuan et al., 2018; Zhao et al., 2014), leading to an intensified water scarcity in this populated area. In this study, we take a semiarid watershed, the Wudinghe in the middle reaches of the Yellow River basin, as a test bed, aiming to solve the following questions: (1) how do hydrological drought characteristics change at different warming levels over the Wudinghe watershed? (2) What are the causes for the hydrological drought change? (3) What are the contributions of uncertainties from different sources (e.g., climate and land surface hydrological models, representative concentration pathway (RCP) scenarios, and internal variability)?

## 2 Study area and dataset

In this study, the Wudinghe watershed was chosen for hydrological drought analysis. As one of the largest subbasins of the Yellow River basin, the Wudinghe watershed is located in the Loess Plateau and has a drainage area of 30 261 km<sup>2</sup> with Baijiachuan hydrological station as the watershed outlet (Fig. 1). It has a semiarid climate with long-term (1956–2010) annual mean precipitation of 356 mm and runoff of 39 mm, resulting in a runoff coefficient of 0.11 (Jiao et al., 2017). Most of the rainfall events are concentrated in summer (June to September) with a large possibility of heavy rains (Mo et al., 2009). Located in the transition zone between cropland–grassland and desert–shrub, the northwest

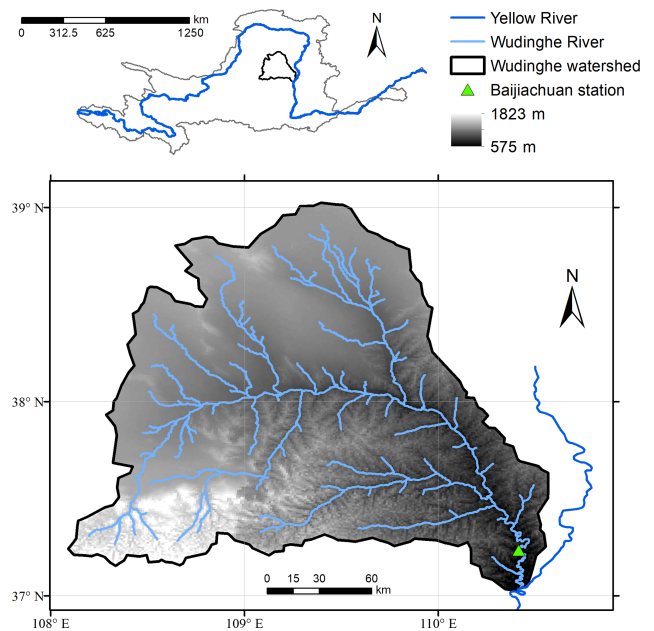


**Figure 1.** Location, elevation and river networks for the Wudinghe watershed.

part of the Wudinghe watershed is dominated by sandy soil, while the major soil type for the southeast part is loess soil. During recent decades, the Wudinghe watershed has experienced a significant streamflow decrease (Yuan et al., 2018; Zhao et al., 2014) and suffered from serious water resource scarcity because of climate change, vegetation degradation and human water consumption (Xiao, 2014; Xu, 2011).

The Coupled Model Intercomparison Project Phase 5 (CMIP5) general circulation model (GCM) simulations for historical experiments and future projections formed the science basis for the IPCC AR5 reports (IPCC, 2014b; Taylor et al., 2012). In this study, we chose eight CMIP5 GCMs for historical (1961–2005) and future (2006–2099) drought analysis, as they provided daily simulations under all four RCP scenarios (i.e. RCP2.6, 4.5, 6.0 and 8.5). Table 1 listed the details of GCMs used in this paper, where historical simulations included all anthropogenic and natural forcings (ALL). Because of the deficiency in GCM precipitation and runoff simulations, we used the corrected meteorological forcing data from CMIP5 climate models to drive a high-resolution land surface hydrological model to simulate runoff and streamflow.

All CMIP5 simulations were bias corrected before being used as land surface model input. After interpolating CMIP5 simulations and China Meteorological Administration (CMA) station observations to the same resolution (0.01° in this study), a modified correction method (Li et al., 2010) based on widely used quantile mapping (Wood et al., 2002; Yuan et al., 2015) was applied to adjust CMIP5/ALL historical simulations and CMIP5/RCP future simulations for each model at each grid cell sepa-

**Table 1.** CMIP5 model simulations used in this study. ALL represents historical simulations with both anthropogenic and natural forcings (r1i1p1 realization), RCP2.6/4.5/6.0/8.5 represent four representative concentration pathways from lower to higher emission scenarios.

GCMs	Institute	Resolution	Historical simulations	RCP scenarios
GFDL-CM3	NOAA GFDL	144 × 90	ALL	RCP2.6/4.5/6.0/8.5
GFDL-ESM2M	NOAA GFDL	144 × 90	ALL	RCP2.6/4.5/6.0/8.5
HadGEM2-ES	MOHC	192 × 145	ALL	RCP2.6/4.5/6.0/8.5
IPSL-CM5A-LR	IPSL	96 × 96	ALL	RCP2.6/4.5/6.0/8.5
IPSL-CM5A-MR	IPSL	144 × 143	ALL	RCP2.6/4.5/6.0/8.5
MIROC-ESM-CHEM	MIROC	128 × 64	ALL	RCP2.6/4.5/6.0/8.5
MIROC-ESM	MIROC	128 × 64	ALL	RCP2.6/4.5/6.0/8.5
MRI-CGCM3	MRI	320 × 160	ALL	RCP2.6/4.5/6.0/8.5

rately. The bias-corrected daily precipitation and temperature were then further temporally disaggregated to a 6 h interval based on the diurnal cycle information from CRUNCEP 6-hourly dataset (<https://svn-ccsm-inputdata.cgd.ucar.edu/trunk/inputdata/atm/datm7/>, last access: 4 September 2016). Other 6-hourly meteorological forcings, i.e., incident solar radiation, air pressure, specific humidity and wind speed, were directly taken from CRUNCEP dataset. Please see Appendix A for details.

### 3 Land surface hydrological model and methods

#### 3.1 Introduction of the CLM-GBHM model

In this study, we chose a newly developed land surface hydrological model, CLM-GBHM, to simulate historical and future streamflow. This model was first developed and applied in the Wudinghe watershed at 0.01° (Jiao et al., 2017) and then the Yellow River basin at 0.05° resolution (Sheng et al., 2017). By improving surface runoff generation, subsurface runoff scheme, river network-based representation and 1-D kinematic wave river routing processes, CLM-GBHM showed good performances in simulating streamflow, soil moisture content and water table depth (Sheng et al., 2017). Figure 2 demonstrated the structure and main ecohydrological processes of CLM-GBHM. Model resolution, surface datasets, initial conditions and model parameters were kept consistent with Jiao et al. (2017), except that monthly LAI in 1982 was used for all simulations because of an unknown vegetation condition in the future.

#### 3.2 Determination of years reaching specific warming levels

IPCC AR5 (IPCC, 2014a) reported that global average surface air temperature change between preindustrial period (1850–1900) and reference period (1986–2005) is 0.61 °C (0.55 to 0.67 °C). Therefore, we took 1986–2005 as the baseline period. Monthly standardized streamflow index (SSI) simulations from CLM-GBHM were com-

pared with the observed records during the baseline period, and the model performed well with a correlative coefficient of 0.53 ( $p < 0.01$ ). Here, “1.5 °C warming level” referred to a global temperature increase of 0.89 °C (= 1.5 – 0.61 °C), “2 °C warming level” referred to an increase of 1.39 °C (= 2 – 0.61 °C), and “3 °C warming level” referred to an increase of 2.39 °C (= 3 – 0.61 °C) compared with the baseline, respectively. As large differences existed in temperature simulations among CMIP5 models and RCP scenarios, we applied a widely used time sampling method (James et al., 2017; Mohammed et al., 2017; Marx et al., 2018) to each GCM under each RCP scenario (referred to as GCM–RCP combination hereafter). A 20-year moving window, which has the same length of the baseline period, was used to determine the first period reaching a specific warming level for each combination, with the period median year referred to as the “crossing year”.

#### 3.3 Identification of hydrological drought characteristics

We used a two-step method similar to previous studies (Lorenzo-Lacruz et al., 2013; Ma et al., 2015; Yuan et al., 2017) to extract hydrological drought characteristics in this paper. At the first step, a hydrological drought index (SSI) was calculated by fitting monthly streamflow using a probabilistic distribution function (Vicente-Serrano et al., 2012; Yuan et al., 2017). Specifically, for each calendar month, streamflow values in that month during baseline period were collected, arranged, and fitted by using a gamma distribution function. Using the same parameters of the fitted gamma distribution, both baseline (1986–2005) and future (2006–2099) streamflow values in that calendar month were standardized to get SSI values. The procedure was repeated for 12 calendar months, 4 RCP scenarios and 8 GCMs separately. The second step was identification and characterization of hydrological drought events by an SSI threshold method (Yuan and Wood, 2013; Lorenzo-Lacruz et al., 2013; Van Loon and Laaha, 2015). Here, a threshold of –0.8 was selected, which is equivalent to a dry condition with a probability of 20 %.

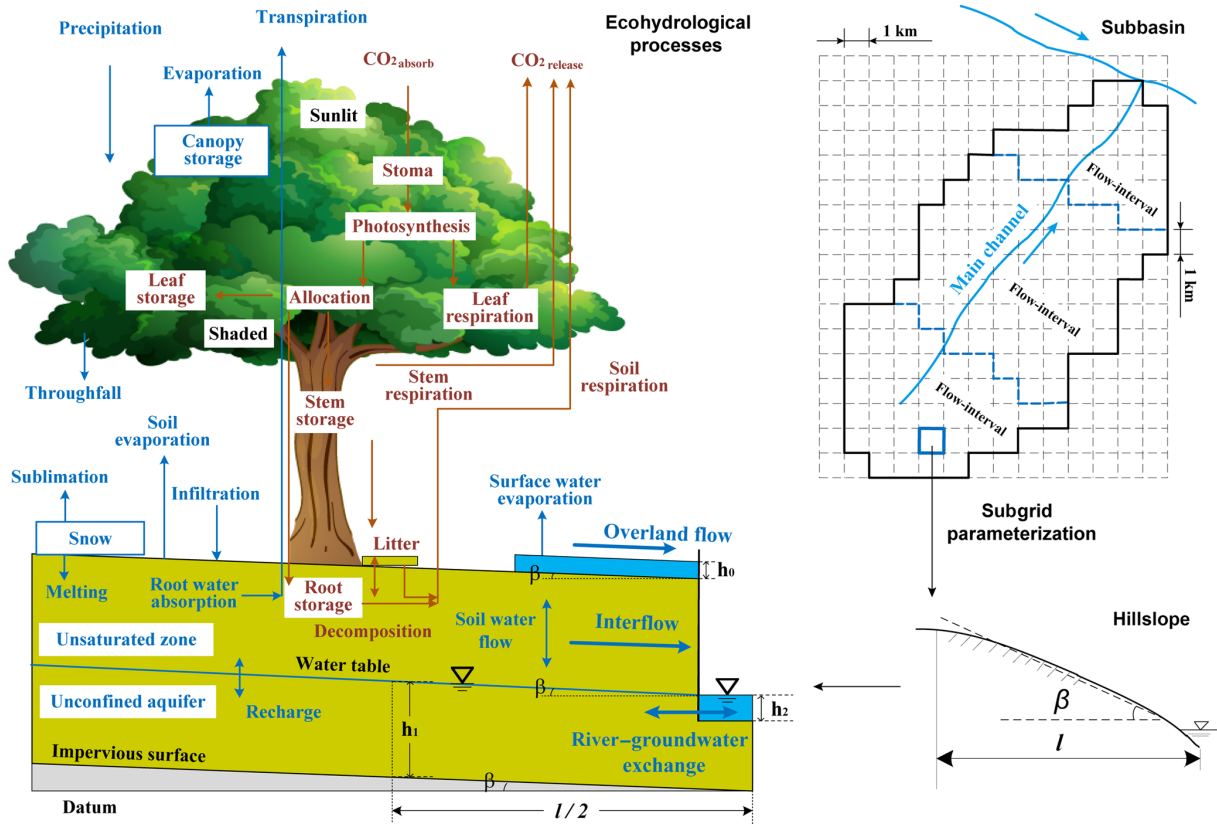


**Figure 2.** Structure and main ecohydrological processes for the land surface hydrological model CLM-GBHM (modified from Jiao et al., 2017).

Months with SSI below  $-0.8$  were treated as dry months, and 3 or more continuous dry months were considered to signify the emergence of a hydrological drought event. To characterize the hydrological drought event, drought duration (months) and severity (sum of the difference between  $-0.8$  and SSI) for a certain drought event were calculated. As future SSI values were all calculated based on historical values, it is important to mention that drought analysis here represented those without adaptation (Samaniego et al., 2018).

### 3.4 Uncertainty separation

Given large spreads among future projections (including combinations of eight GCMs and four RCP scenarios, as shown in shaded areas in Fig. 3), a separation method (Hawkins and Sutton, 2009; Orłowsky and Seneviratne, 2013) was applied to explore uncertainty from three individual sources, i.e., internal variability, climate models and RCP scenarios. In order to separate internal variability from the other two factors with long-term trends, a fourth-order polynomial was selected to fit specific time series: the fitting was first carried out during baseline period (1986–2005) to obtain an average  $i_m$  as a reference value, and then during the future period (2006–2099) to obtain a smooth fit  $x_{m,s,t}$ . Future projections ( $X_{m,s,t}$ ) were then separated into three parts:

reference value ( $i_m$ ), smooth fit ( $x_{m,s,t}$ ) and residual ( $e_{m,s,t}$ ), and the uncertainties from three sources were then calculated as follows:

$$V = \sum_m \text{var}_{s,t}(e_{m,s,t}) / N_m \tag{1}$$

$$M_t = \sum_s \text{var}_m(x_{m,s,t}) / N_s \tag{2}$$

$$S_t = \text{var}_s \left( \sum_m x_{m,s,t} / N_m \right) \tag{3}$$

where  $V$ ,  $M_t$  and  $S_t$  represent uncertainties from internal variability (which is time-invariant), climate models and RCP scenarios;  $N_m$  and  $N_s$  are numbers of climate models and RCP scenarios;  $\text{var}_{s,t}$  denotes the variance across scenarios and time; and  $\text{var}_m$  and  $\text{var}_s$  are variances across models and scenarios respectively. Finally, uncertainty contributions from each component were calculated as proportions to the sum. In this study, we applied this method to the 20-year moving-averaged ensemble time series.

**Table 2.** Trends in hydrometeorological variables and hydrological drought frequency over the Wudinghe watershed. Historical observed trends for streamflow and drought frequency were calculated by using naturalized streamflow data (Yuan et al., 2017). Here, “\*\*” and “\*\*\*” indicate 90 % and 99 % confidence levels, respectively, while those without any “\*\*” show no significant changes ( $p > 0.1$ ).

Historical (1961–2005) and future (2006–2099) scenarios	Changing trend of standardized time series ( $\text{yr}^{-1}$ )			
	Temperature	Precipitation	Streamflow	Drought frequency
Historical observations	0.0494**	−0.0216*	−0.0503**	0.0448**
Historical ALL forcing simulations	0.0272**	−0.0009	−0.0213**	0.0346**
Future RCP2.6 simulations	0.0138**	0.0025*	0.0046**	−0.0069**
Future RCP4.5 simulations	0.0291**	0.0056**	0.0105**	−0.0096**
Future RCP6.0 simulations	0.0312**	0.0039**	0.0038**	−0.0044**
Future RCP8.5 simulations	0.0345**	0.0108**	0.0133**	−0.0107**

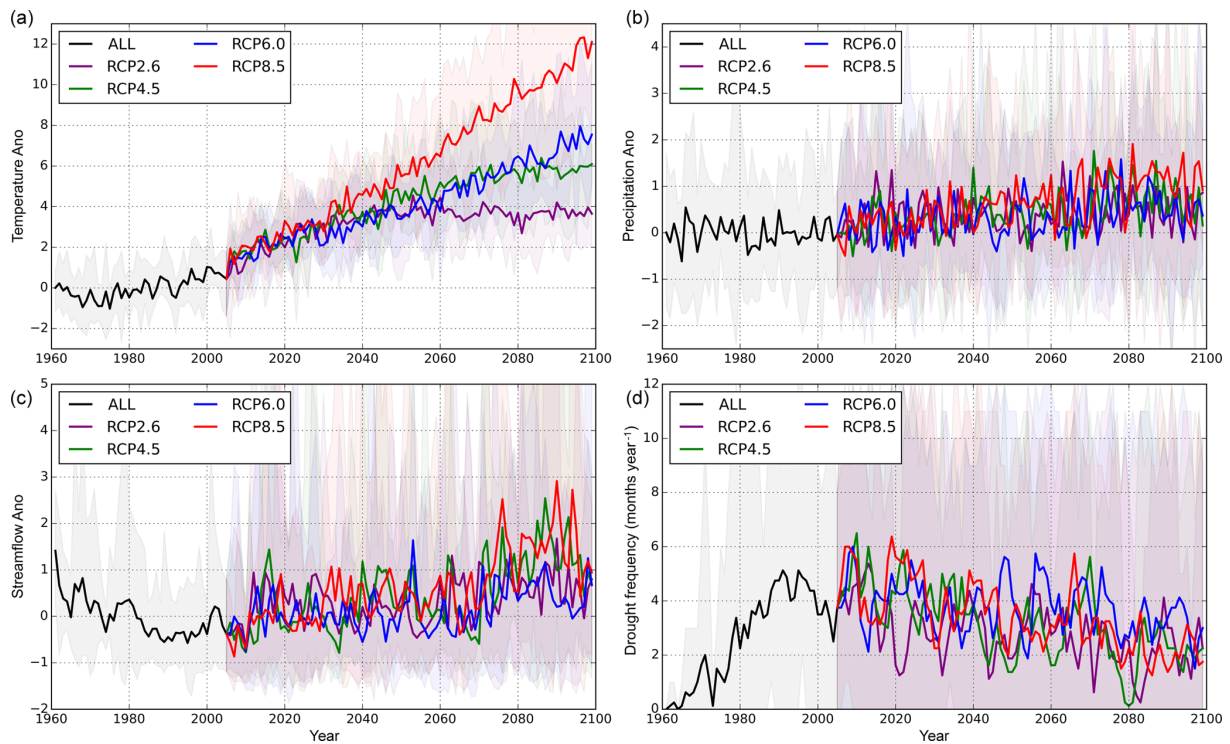


**Figure 3.** Historical (ALL) and future (RCP2.6, 4.5, 6.0 and 8.5) time series of standardized annual mean (a) temperature, (b) precipitation and (c) streamflow, and (d) the time series of hydrological drought frequency (drought months for each year) over the Wudinghe watershed. Shaded areas indicate the ranges between maximum and minimum values among CMIP5/CLM-GBHM model simulations. ALL represents historical simulations with both anthropogenic and natural forcings, RCP2.6, 4.5, 6.0 and 8.5 represent four representative concentration pathways from lower to higher emission scenarios.

## 4 Results

### 4.1 Changes in hydrometeorology in the past and future

We first calculated the trends during both the historical and future periods for basin-averaged annual mean hydrological variables (Table 2 and Fig. 3). During 1961–2005, there was a significant increasing trend ( $p < 0.01$ ) in observed temperature and a decreasing trend ( $p < 0.1$ ) in observed pre-

cipitation, resulting in a decreasing naturalized streamflow ( $p < 0.01$ ) and an increasing hydrological drought frequency ( $p < 0.01$ ). Here, the naturalized streamflow was obtained by adding human water use back to the observed streamflow (Yuan et al., 2017). These historical changes could be captured by hydroclimate model simulations to some extent, although both the warming and drying trends were underestimated (Table 2). Ensemble monthly SSI series from GCM-driven model simulations were also compared with

offline results (CRUNCEP-driven) during the historical period, resulting in a correlative coefficient of 0.47 ( $p < 0.01$ ). During 2006–2099, four variables show consistent changing trends across RCP scenarios, but with different magnitudes (Table 2). Future temperature and precipitation will increase, resulting in an increasing streamflow and decreasing hydrological drought frequency. Unlike temperature trends that increase from RCP2.6 to RCP8.5 (which indicates different radiative forcings), the precipitation trend under RCP6.0 is smaller than that under RCP4.5, suggesting a nonlinear response of the regional water cycle to the increase in radiative forcings. As a result, RCP6.0 shows the smallest increasing rate in streamflow and decreasing rate in drought frequency.

More details could be found in Fig. 3 when focusing on dynamic changes in the history and future. Figure 3a shows that the differences in temperature among RCPs are negligible until the 2030s, when RCP8.5 starts to outclass other scenarios, and the others begin to diverge in the far future (2060s–2080s). In contrast, differences in future precipitation are small throughout the 21st century, except that the RCP8.5 scenario becomes larger after the 2080s (Fig. 3b). As comprehensive outcomes of climate and ecohydrological factors, a clear decrease–increase pattern in streamflow and an increase–decrease trend in hydrological drought frequency are found (Fig. 3c and d). However, differences among RCPs are not discernible. Figure 3b–d also shows that the differences in water-related variables among climate models are very large.

Using the time-sampling method mentioned in Sect. 3.2, the first 20-year periods with mean temperature increasing across 1.5, 2 and 3 °C warming levels for each GCM–RCP combination were identified and listed in Table 3. To demonstrate the overall situation for a specific warming level, we chose the median year among GCMs as the model ensemble for each RCP scenario, and the median year among all GCMs and RCPs as the total ensemble. GCM–RCP combinations not reaching specific warming levels were marked as “NR” in Table 3 and were not considered when calculating the ensemble year.

As listed in Table 3, crossing years for most GCM–RCP combinations reaching 1.5 °C warming level are before 2032, except for GFDL-ESM2M and MRI-CGCM3. Model ensemble years for different RCP scenarios have small differences, and total ensemble year for all GCMs and RCPs is 2025, indicating that 1.5 °C warming level would be reached within 2015–2034. As for 2 and 3 °C warming levels, the total ensemble years are 2042 and 2070, respectively. There are large differences in crossing years among different GCMs, ranging from 2016 to 2075 for 1.5 °C, 2030 to 2076 for 2 °C and 2051 to 2086 for 3 °C. Generally, three global warming thresholds would be reached, first under RCP8.5 and last under the RCP6.0 scenario. None of the GCMs will reach 3 °C warming level under RCP2.6, while under other RCP scenarios this temperature increase would probably be reached around 2073 or even as early as 2050s.

**Table 3.** Determination of crossing year for the periods reaching 1.5, 2 and 3 °C warming levels for different GCM and RCP combinations. Here, “NR” means that the corresponding GCM–RCP combination will not reach the specified warming level throughout the 21st century.

GCMs	1.5 °C warming level						2 °C warming level						3 °C warming level					
	RCP2.6	RCP4.5	RCP6.0	RCP8.5	RCP2.6	RCP4.5	RCP6.0	RCP8.5	RCP2.6	RCP4.5	RCP6.0	RCP8.5	RCP2.6	RCP4.5	RCP6.0	RCP8.5		
GFDL-CM3	2016	2018	2019	2018	2039	2032	2030	NR	2066	2070	2052							
GFDL-ESM2M	NR	2051	2059	2038	NR	NR	2054	NR	NR	NR	2084							
HadGEM2-ES	2020	2023	2023	2018	2042	2039	2032	NR	2071	2070	2052							
IPSL-CM5A-LR	2030	2029	2031	2025	NR	2045	2037	NR	NR	NR	2057							
IPSL-CM5A-MR	2032	2025	2031	2024	NR	2045	2037	NR	NR	NR	2055							
MIROC-ESM-CHEM	2019	2024	2026	2020	2037	2038	2032	NR	2075	2070	2051							
MIROC-ESM	2026	2025	2032	2024	2048	2039	2033	NR	2080	2076	2056							
MRI-CGCM3	2075	2043	2053	2036	NR	2074	2049	NR	NR	NR	2072							
Model ensemble	2026	2025	2031	2024	2041	2039	2035	NR	2073	2073	2056							
Total ensemble	2025 (2016–2075)						2042 (2030–2076)						2070 (2051–2086)					

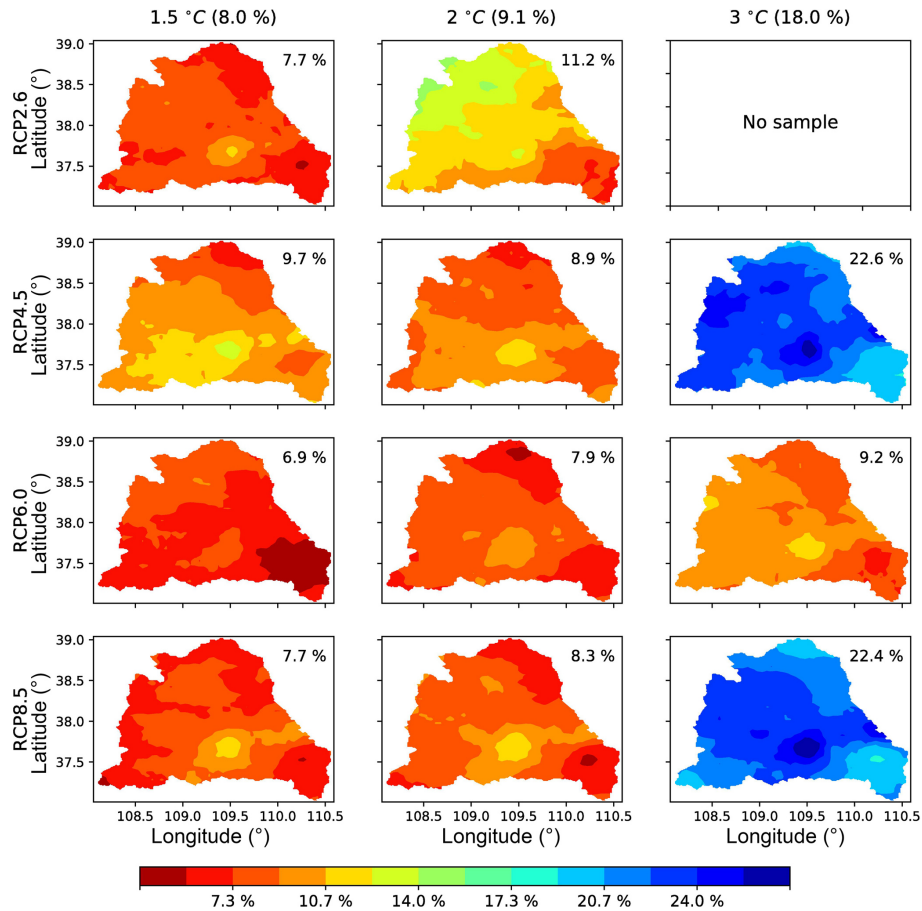


**Figure 4.** Spatial pattern of relative changes in multi-model ensemble mean precipitation at 1.5, 2 and 3 °C warming levels compared to the baseline period (1986–2005). The percentages in the upper-right corners of each panel are the watershed-mean changes for different RCP scenarios, and the percentages in the top brackets are the mean values of all four RCP scenarios.

#### 4.2 Hydrological changes at 1.5, 2 and 3 °C warming levels

After identifying the time periods reaching specific warming levels, we collected precipitation and runoff data within these periods (different among GCM–RCP combinations) and calculated their relative changes compared to the baseline period (1986–2005). Figure 4 shows the spatial pattern of relative changes in model ensemble mean precipitation of these time periods, except for the period under RCP2.6 at 3 °C warming level during which no sample exists. Results indicate that precipitation will increase at all warming levels and all RCP scenarios, while differences exist in spatial patterns. The ensemble mean precipitation increases by 8.0 %, 9.1 % and 18.0 % at 1.5, 2 and 3 °C warming levels for all RCP scenarios respectively, indicating a larger increase in precipitation when warming level increases. For each warming level, precipitation changes among all RCP scenarios are quite close, except for RCP6.0 at 3 °C warming level. Larger precipitation increases generally occur in the south

and southwest parts which are upstream regions of the Wudinghe watershed.

The watershed-mean runoff increases by 26.7 %, 18.7 % and 44.5 % at each warming level respectively, which are larger than those of precipitation because of nonlinear hydrological response (Fig. 5). For all warming levels, RCP8.5 shows greatest runoff increase and RCP2.6 or 6.0 the lowest. Small or negative changes in runoff emerge in the north and southeast regions under RCP2.6, 4.5 and 6.0 scenarios (Fig. 5), where precipitation increases the least (Fig. 4). Besides, runoff changes are also closely linked to watershed river networks, with large increases in the south and middle parts (upper and middle reaches) and small increases or even decreases in the southeast and northeast parts (lower reaches), showing the redistribution effect of surface topography and soil property.

Figure 6 shows the characteristics of hydrological droughts during baseline period and the periods reaching all warming levels. The number of hydrological drought events averaged among all RCP scenarios and climate models is 7 in the baseline period, and it drops to 6.2 (–11 % rela-

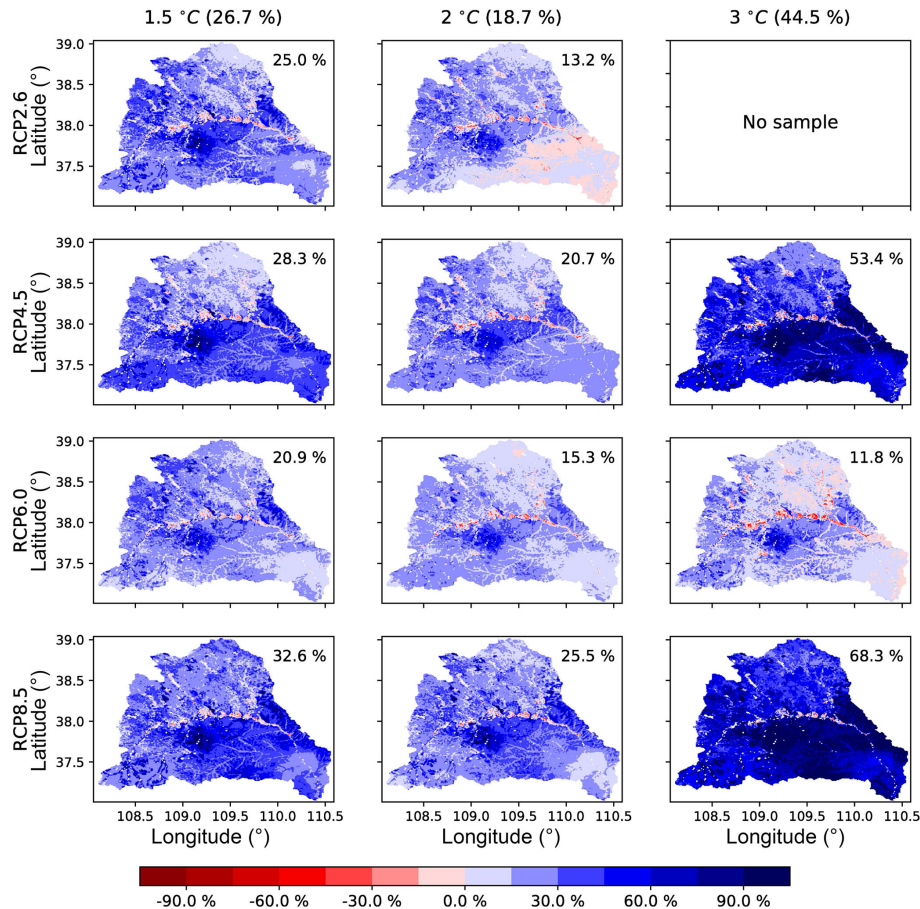


**Figure 5.** The same as Fig. 4, but for the spatial patterns of runoff changes.

tive to baseline, the same below) at 1.5°C, 5.2 (−26 %) at 2°C and 5.4 (−23 %) at 3°C warming levels (Fig. 6a). However, hydrological drought duration increases from 5 months at baseline to 6.5 (+30 %), 5.9 (+18 %) and 6 months (+20 %) at 1.5, 2 and 3°C warming levels, respectively. Drought severity increases dramatically from 1.9 at baseline to 5.4 (+184 %) at 1.5°C warming level and then drops to 4.1 (+116 %) at 2°C warming level and rebounds to 5.4 (+184 %) at 3°C warming level (Fig. 6a). These results indicate that although precipitation and runoff increase, the Wudinghe watershed would suffer from more severe hydrological events in the near future at 1.5°C warming level. The severity could be alleviated in time periods reaching 2°C warming level, with more precipitation occurring over the watershed.

The analysis on individual scenarios suggests a similar conclusion (Fig. 6b–e). Generally, drought amount and severity increase when radiative forcing increases. The least changes in drought severity are found under the RCP4.5 scenario while the largest changes are under the RCP6.0 scenario. Higher warming levels could lead to more moderate drought events under low-emission scenarios (RCP2.6 and 4.5) because of more precipitation in the near future, while

high emissions (RCP6.0 and 8.5) would increase the risk of hydrological drought significantly.

## 5 Discussion

To explore the reason for less frequent but more severe hydrological droughts, we compared the differences in monthly precipitation; evapotranspiration; total, surface and subsurface runoff; and streamflow between the baseline period and periods reaching 1.5, 2 and 3°C warming levels. Standardized indices for these hydrological variables were used to remove seasonality from monthly time series, and mean values and variabilities of these indices were chosen as indicators.

Figure 7 shows that mean values increase as temperature increases for all standardized hydrological indices, showing a wetter hydroclimate in the future, with more precipitation, evapotranspiration, runoff and streamflow (Fig. 7a). However, variabilities for the standardized indices in the future are much higher than those during baseline period, indicating larger fluctuations and higher chance of extreme droughts and floods at all warming levels (Fig. 7b). For extreme drought events (with an SSI < −1.3, representing a

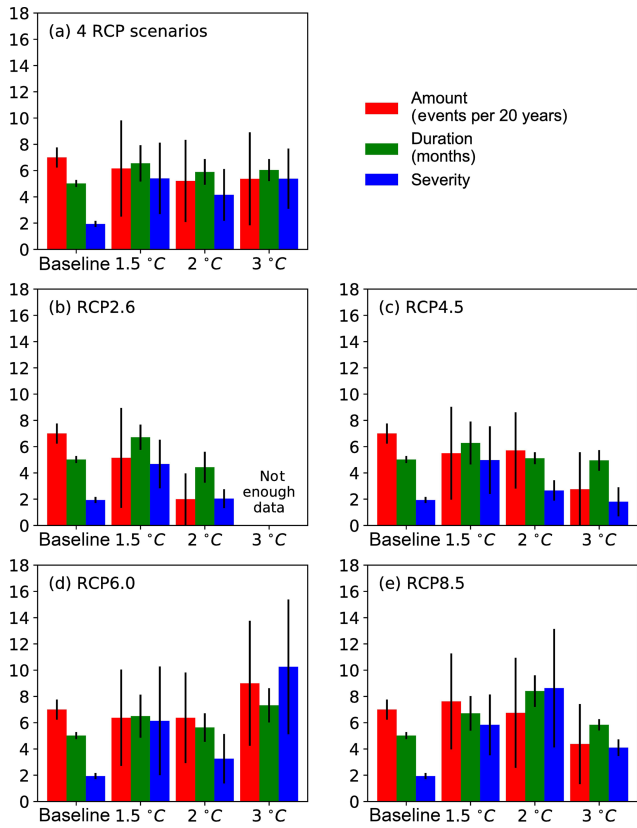


**Figure 6.** Comparison of the characteristics (amount: number of drought events per 20 years; duration: months; and severity) averaged among climate models and RCP scenarios for hydrological drought events during the baseline period (1986–2005) and the periods reaching 1.5, 2 and 3 °C warming levels. Black lines indicate 5%–95% confidence intervals.

dry condition with a probability of 10%), the ensemble mean amounts of drought events are 4.3, 3.1 and 3.7 at 1.5, 2 and 3 °C warming levels, which are much larger than the baseline period with 0.9 (not shown). Focusing on the gaps between baseline and future periods, it is clear that the differences in both evapotranspiration and runoff are larger than those of precipitation for mean values and standard deviations, suggesting the water redistribution through complicated hydrological processes. The increase in the mean value of runoff and consequently streamflow mainly comes from the increase in subsurface runoff. As hydrological drought defined in this paper is based on monthly SSI series, increases in both mean value and variability in precipitation and evapotranspiration indicate a period with less frequent but more severe hydrological drought events.

Another issue is the reliability of results considering large differences among CMIP5 models. Figure 8 shows the uncertainty fractions contributed from internal variability, climate models and RCP scenarios based on multi-model and multi-scenario ensemble projections of temperature, precipitation, streamflow and drought frequency. Uncertainty in tempera-

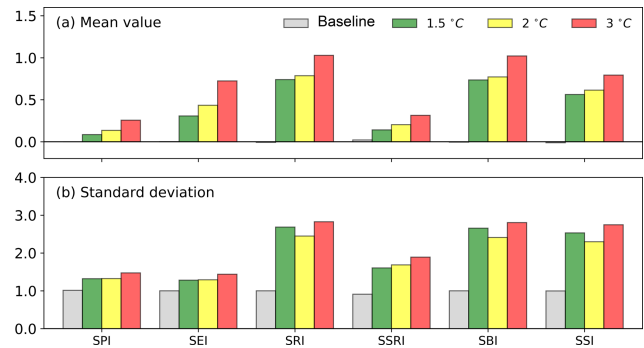


**Figure 7.** Comparison of (a) mean values and (b) standard deviations for hydrological indices averaged among climate models and RCP scenarios during the baseline period (1986–2005) and the periods reaching 1.5, 2 and 3 °C warming levels. SPI, SEI, SRI, SSRI, SBI and SSI represent standardized indices of precipitation, evapotranspiration, runoff, surface runoff, baseflow (subsurface runoff) and streamflow, respectively.

ture projection is mainly contributed by climate models before 2052, and it is then taken over by RCP scenarios. Internal variability contributes to less than 1.5% of the uncertainty for the temperature projection (Fig. 8a). For precipitation projection, climate models account for a large proportion of uncertainty throughout the century. The internal variability contributes to larger uncertainty than RCP scenarios until the second half of the 21st century (Fig. 8b). Similar to precipitation, a major source of uncertainty for the projections of streamflow and hydrological drought frequency is the climate and land surface hydrological models, while the impacts of both internal variability and RCP scenarios are further weakened (Fig. 8c and d).

Generally for all variables except temperature, GCMs and land surface hydrological model account for over 80% of total uncertainties, while internal variability contributes to a comparable or larger proportion than RCP scenarios. RCP scenario only contributes to around 5% of the uncertainties in the projections of streamflow and hydrological drought frequency. These results indicate that the improvement in GCM-simulated precipitation would largely narrow the uncertainties for future projections of hydrological droughts. Besides, previous studies (Marx et al., 2018; Samaniego et al., 2018) have shown that uncertainties contributed from land surface hydrological models can be comparable to that from GCMs, indicating the importance of introducing multiple land surface hydrological models into the analysis of uncertainty, and the significance of exploring more suitable methods in further studies.

There are also some issues for further investigations. As shown in Fig. 3, GCM historical simulations underestimate the increasing trend in temperature and decreasing trend in precipitation and results in underestimations of hydrological drying trends. Although the quantile mapping method used in this study is able to remove the biases in GCM simu-

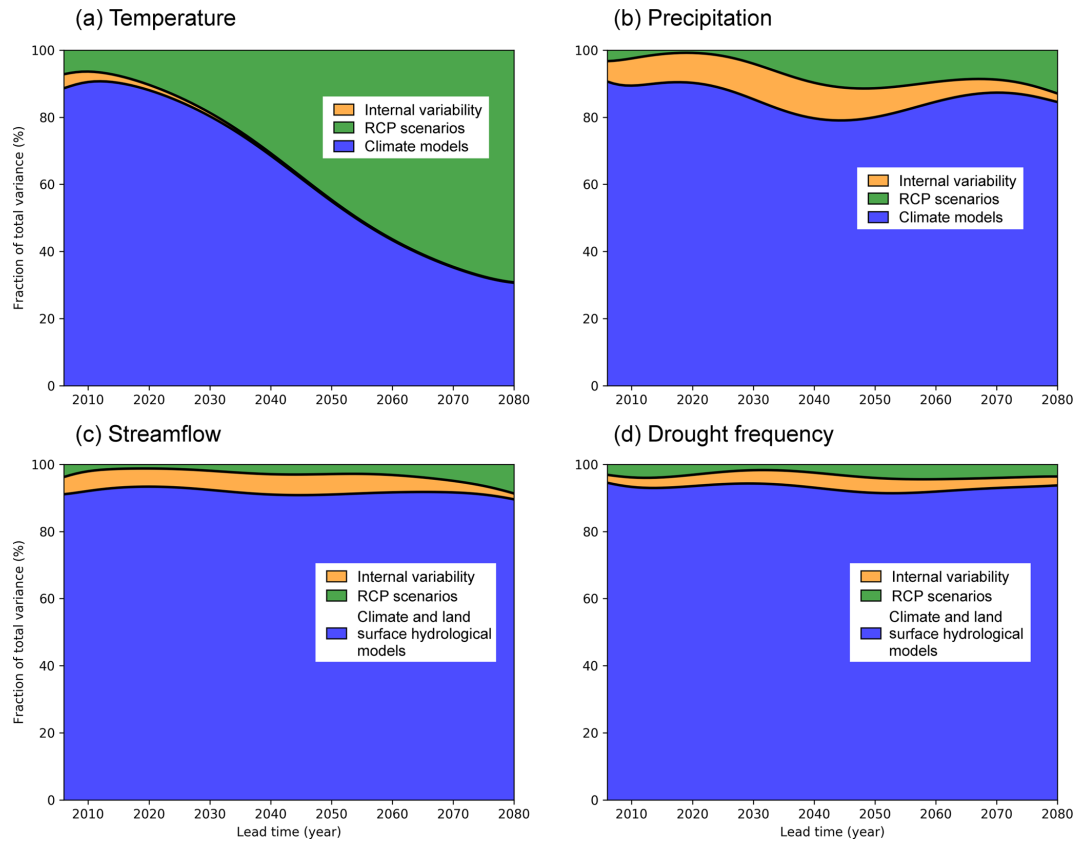


**Figure 8.** Fractions of uncertainties from internal variability (orange), RCP scenarios (green), and climate and land surface hydrological models (blue) for the projections of 20-year moving-averaged (a) temperature, (b) precipitation, (c) streamflow and (d) hydrological drought frequency.

lations (e.g., mean value, variance), the underestimation of trends could not be corrected. An alternative method is to use regional climate models for dynamical downscaling, which would be useful if regional forcings (e.g., topography, land use change, aerosol emission) are strong. Another issue is the spatially varied warming rates. IPCC AR5 reported (IPCC, 2014c) that global warming for the last 20 years compared to the preindustrial period are 0.3–1.7 °C (RCP2.6), 1.1–2.6 °C (RCP4.5), 1.4–3.1 °C (RCP6.0) and 2.6–4.8 °C (RCP8.5). However, temperature increases vary a lot for different regions. For instance, temperature rises faster in high-altitude (Kraaijenbrink et al., 2017) and polar regions (Bromwich et al., 2013), where the rate of regional warming could be 3 times that of global warming. Actually, reaching periods for regional warming thresholds in the Wudinghe watershed are earlier than the global ones (not shown here), which suggest that the regional warming would be more severe at specific global warming levels.

## 6 Conclusions

In this paper, we bias-corrected future projections of meteorological forcings from eight CMIP5 GCM simulations under four RCP scenarios to drive a newly developed land surface hydrological model, CLM-GBHM, to project changes in streamflow and hydrological drought characteristics over the Wudinghe watershed. After determining the time periods reaching 1.5, 2 and 3 °C global warming levels for each GCM–RCP combination, we focused on the changes in regional hydrological drought characteristics at all warming levels. Moreover, projection uncertainties from different sources were separated and analyzed. The main conclusions are listed as follows:

1. With CMIP5 GCM simulations as forcing data, the model ensemble mean hindcast can reproduce the significant decreasing trend of streamflow and increasing trend of hydrological drought frequency in the historical period (1961–2005), but the drying trend is underestimated because of GCM uncertainties. Streamflow increases and hydrological drought frequency decreases in the future under all RCP scenarios.

2. The time periods reaching 1.5, 2 and 3 °C warming levels over the Wudinghe watershed are 2015–2034, 2032–2051 and 2060–2079, respectively. There are large differences in results among different GCMs, while different RCP scenarios show consistence in reaching periods, with RCP8.5 the earliest and RCP6.0 the latest.
3. Precipitation increases under all RCP scenarios at all warming levels (8 %, 9 % and 18 %), while differences exist in spatial patterns. Runoff has larger relative change rates (27 %, 19 % and 44 %), while larger increases in runoff occurred in the upper and middle reaches and fewer increases or even decreases emerged in the lower reaches, indicating a complex spatial distribution in hydrological droughts.
4. As a result of increasing mean values and variability for precipitation, evapotranspiration and runoff, hydrological drought frequency drops by 11 %–26 % at all warming levels compared to the baseline period, while hydrological drought severity rises dramatically by 116 %–184 %. This indicates that the Wudinghe watershed would suffer more severe hydrological drought events in the future, especially under RCP6.0 and RCP8.5 scenarios.
5. The main uncertainty sources vary among hydrological variables. Most uncertainties are from climate and land surface models, especially for precipitation. At all warming levels, models contribute to over 80 % of total uncertainties, while internal variability contributes to a comparable proportion of uncertainties to RCP scenarios for precipitation, streamflow and hydrological drought frequency.

*Data availability.* CMIP5 daily precipitation and temperature simulations from eight GCMs were collected from the CMIP5-DKRZ data site powered by ESGF and CoG: <https://esgf-data.dkrz.de/search/cmip5-dkrz> (Taylor et al., 2012). CRUNCEP (version 4) 6-hourly atmospheric forcing data were obtained from NCAR's Climate and Global Dynamics Laboratory website: <https://svn-ccsm-inputdata.cgd.ucar.edu/trunk/inputdata/atm/dtm7> (Piao et al., 2012). Daily station observations for bias correction were obtained from the China National Meteorological Information Center website: [http://data.cma.cn/en/?r=data/detail&dataCode=SURF\\_CLI\\_CHN\\_MUL\\_DAY\\_CES\\_V3.0](http://data.cma.cn/en/?r=data/detail&dataCode=SURF_CLI_CHN_MUL_DAY_CES_V3.0) (Shen et al., 2014).

## Appendix A: Details of processing climate forcings

The land surface hydrological model CLM-GBHM requires a list of input climate forcings, i.e. precipitation, near-surface air temperature, incident solar radiation, air pressure, specific humidity and wind speed. These variables were generated from three datasets in this study: CMIP5 daily simulations during both historical (1961–2005) and future (2006–2099) periods, CRUNCEP 6-hourly dataset during 1959–2005, and China Meteorological Administration (CMA) daily station observations during 1961–2005. All datasets were firstly re-gridded to the same resolution ( $0.01^\circ$ ) by using a bilinear interpolation method for further processing.

After spatial interpolation, daily precipitation and temperature from CMIP5 simulations were adjusted to remove their monthly biases compared to CMA observations, by applying a correction method to each model at each grid cell separately. This method modified the widely used quantile-mapping method (CDFm) and processed historical and future time series in different ways. For the historical period, the bias-corrected monthly variable  $x$  (i.e., precipitation or temperature) was calculated based on CDFm:

$$x_{\text{sim,his,corrected}} = F_{\text{obs,his}}^{-1} \left( F_{\text{sim,his}} \left( x_{\text{sim,his,based}} \right) \right), \quad (\text{A1})$$

where  $F$  is the cumulative distribution function of variable  $x$ , subscripts “sim”, “obs”, “his”, “biased” and “corrected” represent simulated value, observed value, historical period, value with bias and value after bias correction at monthly scale, respectively. The basic assumption of CDFm is that the climate distribution does not change much over time; however, this is invalid considering intense global warming in the future. Therefore, an equidistant CDF matching method (EDCDFm; Li et al., 2010) was applied for future projections, which assumes that the difference between simulated and observed values remains the same over time:

$$x_{\text{sim,fut,corrected}} = x_{\text{sim,fut,based}} + F_{\text{obs,his}}^{-1} \left( F_{\text{sim,fut}} \left( x_{\text{sim,fut,based}} \right) \right) - F_{\text{sim,his}}^{-1} \left( F_{\text{sim,fut}} \left( x_{\text{sim,fut,based}} \right) \right), \quad (\text{A2})$$

where the subscript “fut” represents future period. After bias correction at monthly scale, new daily precipitation (temperature) series were generated based on the ratio (difference) between the new and old CMIP5 simulated monthly means:

$$P_{\text{d,corrected}} = \left( P_{\text{m,corrected}} / P_{\text{m,based}} \right) \cdot P_{\text{d,based}}, \quad (\text{A3})$$

$$T_{\text{d,corrected}} = \left( T_{\text{m,corrected}} - T_{\text{m,based}} \right) + T_{\text{d,based}}, \quad (\text{A4})$$

where  $P$  and  $T$  represent precipitation and temperature, and subscripts “d” and “m” represent daily value and corresponding monthly mean, respectively.

In order to temporally disaggregate daily temperature and precipitation to a 6 h interval during both historical and future periods, the diurnal cycle information from CRUNCEP dataset was introduced. By looping the CRUNCEP data during 1959–2005 (47 years) twice, we could also generate “future data” (2006–2099, 94 years). By using the same disaggregation method that downscales variables from monthly to daily, temporal downscaling from daily to 6-hourly scales was achieved:

$$P_{\text{6h,corrected}} = \left( P_{\text{d,corrected}} / P_{\text{d,CRUNCEP}} \right) \cdot P_{\text{6h,CRUNCEP}}, \quad (\text{A5})$$

$$T_{\text{6h,corrected}} = \left( T_{\text{d,corrected}} - T_{\text{d,CRUNCEP}} \right) + T_{\text{6h,CRUNCEP}}, \quad (\text{A6})$$

where the subscript “6h” represents 6-hourly values. It should be mentioned that only precipitation and temperature have been used from CMIP5 models, with other climate forcing variables (i.e., incident solar radiation, air pressure, specific humidity and wind speed series) directly taken from CRUNCEP dataset. Whether physical consistency among all climate forcing variables was maintained or not by simply introducing CRUNCEP dataset was not considered in this study, and it is unclear how the climate change signals by GCMs might be affected by using CRUNCEP data for a majority of forcing variables. Although resampling methods (e.g., Schaake shuffle) that are widely used in temporal downscaling for seasonal forecasting might result in more consistent forcing variables, whether such consistency (e.g., temperature–humidity relationship) holds for future projection given the changing climate is unknown. More sophisticated downscaling techniques (either statistical or dynamical) are needed for further studies.

*Author contributions.* XY conceived and designed the study. YJ performed the analyses and wrote the paper. XY revised the paper.

*Competing interests.* The authors declare that they have no conflict of interest.

*Acknowledgements.* We would like to thank the editor and two anonymous reviewers for their helpful comments. This research was supported by National Key R & D Program of China (2018YFA0606002), Strategic Priority Research Program of Chinese Academy of Sciences (XDA20020201), and the Startup Foundation for Introducing Talent of NUIST. Daily precipitation and temperature simulated by CMIP5 models were provided by the World Climate Research Programme's Working Group on Coupled Modeling (<https://esgf-data.dkrz.de/search/cmip5-dkrz>, last access: 26 May 2017). We thank Dawen Yang and Huimin Lei for the implementation of the CLM-GBHM land surface hydrological model.

Edited by: Micha Werner

Reviewed by: Bin Peng and one anonymous referee

## References

- Barnett, T. P., Adam, J. C., and Lettenmaier, D. P.: Potential impacts of a warming climate on water availability in snow-dominated regions, *Nature*, 438, 303–309, <https://doi.org/10.1038/nature04141>, 2005.
- Bromwich, D. H., Nicolas, J. P., Monaghan, A. J., Lazzara, M. A., Keller, L. M., Weidner, G. A., and Wilson, A. B.: Central West Antarctica among the most rapidly warming regions on Earth, *Nat. Geosci.*, 6, 139–145, <https://doi.org/10.1038/Ngeo1671>, 2013.
- Chang, J., Li, Y., Wang, Y., and Yuan, M.: Copula-based drought risk assessment combined with an integrated index in the Wei River Basin, China, *J. Hydrol.*, 540, 824–834, <https://doi.org/10.1016/j.jhydrol.2016.06.064>, 2016.
- Dai, A. G.: Drought under global warming: a review, *Wires Clim. Change*, 2, 45–65, <https://doi.org/10.1002/wcc.81>, 2011.
- Gitay, H., Suárez, A., Watson, R. T., and Dokken, D. J.: Climate change and biodiversity, IPCC Technical Paper V, IPCC, Geneva, 2002.
- Hawkins, E., and Sutton, R.: The Potential to Narrow Uncertainty in Regional Climate Predictions, *B. Am. Meteorol. Soc.*, 90, 1095, <https://doi.org/10.1175/2009bams2607.1>, 2009.
- IPCC: Climate Change 2013 – The Physical Science Basis, Cambridge University Press, Cambridge, UK and New York, NY, USA, 1535 pp., 2014a.
- IPCC: Summary for Policymakers, in: Climate Change 2013 – The Physical Science Basis, edited by: Stocker, T. F., Qin, D., Plattner, G.-K., Tignor, M., Allen, S. K., Boschung, J., Nauels, A., Xia, Y., Bex, V., and Midgley, P. M., Cambridge University Press, Cambridge, UK and New York, NY, USA, 1–30, 2014b.
- IPCC: Long-term Climate Change: Projections, Commitments and Irreversibility, in: Climate Change 2013 – The Physical Science Basis, edited by: Stocker, T. F., Qin, D., Plattner, G.-K., Tignor, M., Allen, S. K., Boschung, J., Nauels, A., Xia, Y., Bex, V., and Midgley, P. M., Cambridge University Press, Cambridge, UK and New York, NY, USA, 1029–1136, 2014c.
- James, R., Washington, R., Schleussner, C. F., Rogelj, J., and Conway, D.: Characterizing half-a-degree difference: a review of methods for identifying regional climate responses to global warming targets, *Wires Clim. Change*, 8, e457, <https://doi.org/10.1002/wcc.457>, 2017.
- Jiao, Y., Lei, H. M., Yang, D. W., Huang, M. Y., Liu, D. F., and Yuan, X.: Impact of vegetation dynamics on hydrological processes in a semi-arid basin by using a land surface-hydrology coupled model, *J. Hydrol.*, 551, 116–131, <https://doi.org/10.1016/j.jhydrol.2017.05.060>, 2017.
- Kormos, P. R., Luce, C. H., Wenger, S. J., and Berghuijs, W. R.: Trends and sensitivities of low streamflow extremes to discharge timing and magnitude in Pacific Northwest mountain streams, *Water Resour. Res.*, 52, 4990–5007, <https://doi.org/10.1002/2015wr018125>, 2016.
- Kraaijenbrink, P. D. A., Bierkens, M. F. P., Lutz, A. F., and Immerzeel, W. W.: Impact of a global temperature rise of 1.5 °C on Asia's glaciers, *Nature*, 549, 257–260, <https://doi.org/10.1038/nature23878>, 2017.
- Li, H. B., Sheffield, J., and Wood, E. F.: Bias correction of monthly precipitation and temperature fields from Intergovernmental Panel on Climate Change AR4 models using equidistant quantile matching, *J. Geophys. Res.-Atmos.*, 115, D10101, <https://doi.org/10.1029/2009jd012882>, 2010.
- Lorenzo-Lacruz, J., Moran-Tejeda, E., Vicente-Serrano, S. M., and Lopez-Moreno, J. I.: Streamflow droughts in the Iberian Peninsula between 1945 and 2005: spatial and temporal patterns, *Hydrol. Earth Syst. Sci.*, 17, 119–134, <https://doi.org/10.5194/hess-17-119-2013>, 2013.
- Ma, F., Yuan, X., and Ye, A. Z.: Seasonal drought predictability and forecast skill over China, *J. Geophys. Res.-Atmos.*, 120, 8264–8275, <https://doi.org/10.1002/2015jd023185>, 2015.
- Marx, A., Kumar, R., Thober, S., Rakovec, O., Wanders, N., Zink, M., Wood, E. F., Pan, M., Sheffield, J., and Samaniego, L.: Climate change alters low flows in Europe under global warming of 1.5, 2, and 3 °C, *Hydrol. Earth Syst. Sci.*, 22, 1017–1032, <https://doi.org/10.5194/hess-22-1017-2018>, 2018.
- McVicar, T. R., Roderick, M. L., Donohue, R. J., Li, L. T., Van Niel, T. G., Thomas, A., Grieser, J., Jhajharia, D., Himri, Y., Mahowald, N. M., Mescherskaya, A. V., Kruger, A. C., Rehman, S., and Dinpashoh, Y.: Global review and synthesis of trends in observed terrestrial near-surface wind speeds: Implications for evaporation, *J. Hydrol.*, 416, 182–205, <https://doi.org/10.1016/j.jhydrol.2011.10.024>, 2012.
- Mo, X. G., Liu, S. X., Chen, D., Lin, Z. H., Guo, R. P., and Wang, K.: Grid-size effects on estimation of evapotranspiration and gross primary production over a large Loess Plateau basin, China, *Hydrolog. Sci. J.*, 54, 160–173, <https://doi.org/10.1623/hysj.54.1.160>, 2009.
- Mohammed, K., Islam, A. S., Islam, G. M. T., Alfieri, L., Bala, S. K., and Khan, M. J. U.: Extreme flows and water availability of the Brahmaputra River under 1.5 and 2 °C global warming scenarios, *Climatic Change*, 145, 159–175, <https://doi.org/10.1007/s10584-017-2073-2>, 2017.

- Orlowsky, B. and Seneviratne, S. I.: Elusive drought: uncertainty in observed trends and short- and long-term CMIP5 projections, *Hydrol. Earth Syst. Sci.*, 17, 1765–1781, <https://doi.org/10.5194/hess-17-1765-2013>, 2013.
- Parajka, J., Blaschke, A. P., Bloeschl, G., Haslinger, K., Hepp, G., Laaha, G., Schoener, W., Trautvetter, H., Viglione, A., and Zessner, M.: Uncertainty contributions to low-flow projections in Austria, *Hydrol. Earth Syst. Sci.*, 20, 2085–2101, <https://doi.org/10.5194/hess-20-2085-2016>, 2016.
- Perez, G. A. C., van Huijgevoort, M. H. J., Voss, F., and van Lanen, H. A. J.: On the spatio-temporal analysis of hydrological droughts from global hydrological models, *Hydrol. Earth Syst. Sci.*, 15, 2963–2978, <https://doi.org/10.5194/hess-15-2963-2011>, 2011.
- Peters, G. P., Andrew, R. M., Boden, T., Canadell, J. G., Ciais, P., Le Quééré, C., Marland, G., Raupach, M. R., and Wilson, C.: The challenge to keep global warming below 2°C, *Nat. Clim. Change*, 3, 4–6, 2012.
- Piao, S. L., Ito, A., Li, S. G., Huang, Y., Ciais, P., Wang, X. H., Peng, S. S., Nan, H. J., Zhao, C., Ahlstrom, A., Andres, R. J., Chevallier, F., Fang, J. Y., Hartmann, J., Huntingford, C., Jeong, S., Levis, S., Levy, P. E., Li, J. S., Lomas, M. R., Mao, J. F., Mayorga, E., Mohammat, A., Muraoka, H., Peng, C. H., Peylin, P., Poulter, B., Shen, Z. H., Shi, X., Sitch, S., Tao, S., Tian, H. Q., Wu, X. P., Xu, M., Yu, G. R., Viovy, N., Zaehle, S., Zeng, N., and Zhu, B.: The carbon budget of terrestrial ecosystems in East Asia over the last two decades, *Biogeosciences*, 9, 3571–3586, <https://doi.org/10.5194/bg-9-3571-2012>, 2012.
- Prudhomme, C., Giuntoli, I., Robinson, E. L., Clark, D. B., Arnell, N. W., Dankers, R., Fekete, B. M., Franssen, W., Gerten, D., Gosling, S. N., Hagemann, S., Hannah, D. M., Kim, H., Masaki, Y., Satoh, Y., Stacke, T., Wada, Y., and Wisser, D.: Hydrological droughts in the 21st century, hotspots and uncertainties from a global multimodel ensemble experiment, *P. Natl. Acad. Sci. USA*, 111, 3262–3267, <https://doi.org/10.1073/pnas.1222473110>, 2014.
- Rogelj, J., Luderer, G., Pietzcker, R. C., Kriegler, E., Schaeffer, M., Krey, V., and Riahi, K.: Energy system transformations for limiting end-of-century warming to below 1.5°C, *Nat. Clim. Change*, 5, 519–527, <https://doi.org/10.1038/nclimate2572>, 2015.
- Roudier, P., Andersson, J. C. M., Donnelly, C., Feyen, L., Greuell, W., and Ludwig, F.: Projections of future floods and hydrological droughts in Europe under +2°C global warming, *Climatic Change*, 135, 341–355, <https://doi.org/10.1007/s10584-015-1570-4>, 2016.
- Samaniego, L., Thober, S., Kumar, R., Wanders, N., Rakovec, O., Pan, M., Zink, M., Sheffield, J., Wood, E., and Marx, A.: Anthropogenic warming exacerbates European soil moisture droughts, *Nat. Clim. Change*, 8, 421–426, <https://doi.org/10.1038/s41558-018-0138-5>, 2018.
- Shen, Y., Zhao, P., Pan, Y., and Yu, J. J.: A high spatiotemporal gauge-satellite merged precipitation analysis over China, *J. Geophys. Res.-Atmos.*, 119, 3063–3075, <https://doi.org/10.1002/2013JD020686>, 2014.
- Sheng, M. Y., Lei, H. M., Jiao, Y., and Yang, D. W.: Evaluation of the Runoff and River Routing Schemes in the Community Land Model of the Yellow River Basin, *J. Adv. Model. Earth Syst.*, 9, 2993–3018, <https://doi.org/10.1002/2017ms001026>, 2017.
- Tang, Y., Tang, Q., Tian, F., Zhang, Z., and Liu, G.: Responses of natural runoff to recent climatic variations in the Yellow River basin, China, *Hydrol. Earth Syst. Sci.*, 17, 4471–4480, <https://doi.org/10.5194/hess-17-4471-2013>, 2013.
- Taylor, K. E., Stouffer, R. J., and Meehl, G. A.: An Overview of Cmp5 and the Experiment Design, *B. Am. Meteorol. Soc.*, 93, 485–498, <https://doi.org/10.1175/Bams-D-11-00094.1>, 2012.
- Thornton, P. K., Ericksen, P. J., Herrero, M., and Challinor, A. J.: Climate variability and vulnerability to climate change: a review, *Global Change Biol.*, 20, 3313–3328, <https://doi.org/10.1111/gcb.12581>, 2014.
- Tirado, M. C., Clarke, R., Jaykus, L. A., McQuatters-Gollop, A., and Franke, J. M.: Climate change and food safety: A review, *Food Res. Int.*, 43, 1745–1765, <https://doi.org/10.1016/j.foodres.2010.07.003>, 2010.
- Van Loon, A. F. and Laaha, G.: Hydrological drought severity explained by climate and catchment characteristics, *J. Hydrol.*, 526, 3–14, <https://doi.org/10.1016/j.jhydrol.2014.10.059>, 2015.
- Van Loon, A. F., Stahl, K., Di Baldassarre, G., Clark, J., Rango-croft, S., Wanders, N., Gleeson, T., Van Dijk, A. I. J. M., Tallaksen, L. M., Hannaford, J., Uijlenhoet, R., Teuling, A. J., Hannah, D. M., Sheffield, J., Svoboda, M., Verbeiren, B., Wagener, T., and Van Lanen, H. A. J.: Drought in a human-modified world: reframing drought definitions, understanding, and analysis approaches, *Hydrol. Earth Syst. Sci.*, 20, 3631–3650, <https://doi.org/10.5194/hess-20-3631-2016>, 2016.
- Vicente-Serrano, S. M., Lopez-Moreno, J. I., Begueria, S., Lorenzo-Lacruz, J., Azorin-Molina, C., and Moran-Tejeda, E.: Accurate Computation of a Streamflow Drought Index, *J. Hydrol. Eng.*, 17, 318–332, [https://doi.org/10.1061/\(ASCE\)HE.1943-5584.0000433](https://doi.org/10.1061/(ASCE)HE.1943-5584.0000433), 2012.
- Vorosmarty, C. J., Green, P., Salisbury, J., and Lammers, R. B.: Global water resources: Vulnerability from climate change and population growth, *Science*, 289, 284–288, <https://doi.org/10.1126/science.289.5477.284>, 2000.
- Wanders, N. and Wada, Y.: Human and climate impacts on the 21st century hydrological drought, *J. Hydrol.*, 526, 208–220, <https://doi.org/10.1016/j.jhydrol.2014.10.047>, 2015.
- Wood, A. W., Maurer, E. P., Kumar, A., and Lettenmaier, D. P.: Long-range experimental hydrologic forecasting for the eastern United States, *J. Geophys. Res.-Atmos.*, 107, 4429, <https://doi.org/10.1029/2001jd000659>, 2002.
- Xiao, J. F.: Satellite evidence for significant biophysical consequences of the “Grain for Green” Program on the Loess Plateau in China, *J. Geophys. Res.-Biogeo.*, 119, 2261–2275, <https://doi.org/10.1002/2014jg002820>, 2014.
- Xu, J. X.: Variation in annual runoff of the Wudinghe River as influenced by climate change and human activity, *Quatern. Int.*, 244, 230–237, <https://doi.org/10.1016/j.quaint.2010.09.014>, 2011.
- Yuan, X. and Wood, E. F.: Multimodel seasonal forecasting of global drought onset, *Geophys. Res. Lett.*, 40, 4900–4905, <https://doi.org/10.1002/grl.50949>, 2013.
- Yuan, X., Roundy, J. K., Wood, E. F., and Sheffield, J.: Seasonal forecasting of global hydrologic extremes: system development and evaluation over GEWEX basins, *B. Am. Meteorol. Soc.*, 96, 1895–1912, <https://doi.org/10.1175/BAMS-D-14-00003.1>, 2015.
- Yuan, X., Zhang, M., Wang, L. Y., and Zhou, T.: Understanding and seasonal forecasting of hydrological drought in

- the Anthropocene, *Hydrol. Earth Syst. Sci.*, 21, 5477–5492, <https://doi.org/10.5194/hess-21-5477-2017>, 2017.
- Yuan, X., Jiao, Y., Yang, D., and Lei, H.: Reconciling the attribution of changes in streamflow extremes from a hydroclimate perspective, *Water Resour. Res.*, 54, 3886–3895, <https://doi.org/10.1029/2018WR022714>, 2018.
- Zhang, X. P., Zhang, L., Zhao, J., Rustomji, P., and Hairsine, P.: Responses of streamflow to changes in climate and land use/cover in the Loess Plateau, China, *Water Resour. Res.*, 44, W00A07, <https://doi.org/10.1029/2007wr006711>, 2008.
- Zhao, G. J., Tian, P., Mu, X. M., Jiao, J. Y., Wang, F., and Gao, P.: Quantifying the impact of climate variability and human activities on streamflow in the middle reaches of the Yellow River basin, China, *J. Hydrol.*, 519, 387–398, <https://doi.org/10.1016/j.jhydrol.2014.07.014>, 2014.
- Zheng, H. X., Zhang, L., Zhu, R. R., Liu, C. M., Sato, Y., and Fukushima, Y.: Responses of streamflow to climate and land surface change in the headwaters of the Yellow River Basin, *Water Resour. Res.*, 45, W00A19, <https://doi.org/10.1029/2007wr006665>, 2009.
- Zhu, Z. C., Piao, S. L., Myneni, R. B., Huang, M. T., Zeng, Z. Z., Canadell, J. G., Ciais, P., Sitch, S., Friedlingstein, P., Arneth, A., Cao, C. X., Cheng, L., Kato, E., Koven, C., Li, Y., Lian, X., Liu, Y. W., Liu, R. G., Mao, J. F., Pan, Y. Z., Peng, S. S., Penuelas, J., Poulter, B., Pugh, T. A. M., Stocker, B. D., Viovy, N., Wang, X. H., Wang, Y. P., Xiao, Z. Q., Yang, H., Zaehle, S., and Zeng, N.: Greening of the Earth and its drivers, *Nat. Clim. Change*, 6, 791–795, <https://doi.org/10.1038/nclimate3004>, 2016.